J Solid State Electrochem (2012) 16:1841–1848
DOI 10.1007/s10008-011-1566-6

ORIGINAL PAPER

Optimising organic ionic plastic crystal electrolyte for all solid-state and higher than ambient temperature lithium batteries

Jaka Sunarso · Youssof Shekibi · Jim Efthimiadis · Liyu Jin · Jennifer M. Pringle · Anthony F. Hollenkamp · Douglas R. MacFarlane · Maria Forsyth · Patrick C. Howlett

Received: 1 September 2011 / Revised: 26 September 2011 / Accepted: 3 October 2011 / Published online: 26 October 2011

Abstract Organic ionic plastic crystal (OIPC) electrolytes are among the key enabling materials for solid-state and higher than ambient temperature lithium batteries. This work overviews some of the parameter studies on the Li|OIPC interface using lithium symmetrical cells as well as the optimisation and performance of Li|OIPC|$LiFePO_4$ cells. The effects of temperature and electrolyte thickness on the cycle performance of the lithium symmetrical cell, particularly with respect to the interfacial and bulk resistances, are demonstrated. Whilst temperature change substantially alters both the interfacial and bulk resistance, changing the electrolyte thickness predominantly changes the bulk resistance only. In addition, an upper limit of the current density is demonstrated, above which irreversible processes related to electrolyte decomposition take place. Here, we demonstrate an excellent discharge capacity attained on $LiFePO_4$| 10 mol% $LiNTf_2$-doped $[C_2mpyr][NTf_2]$|Li cell, reaching 126 mAh g^{-1} at 50 °C (when the electrolyte is in its solid form) and 153 mAh g^{-1} at 80 °C (when the electrolyte is in its liquid form). Most remarkably, at high temperature operation, the capacity retention at long cycles and high current is excellent with only a slight (3%) drop in discharge capacity upon increasing the current from 0.2 C to 0.5 C. These results highlight the real prospects for developing a lithium battery with high temperature performance that easily surpasses that achievable with even the best contemporary lithium-ion technology.

J. Sunarso · J. Efthimiadis · M. Forsyth · P. C. Howlett (✉)
Australian Research Council (ARC) Centre of Excellence for Electromaterials Science, Institute for Technology Research and Innovation, Deakin University,
221 Burwood Hwy,
Burwood, Victoria 3125, Australia
e-mail: patrick.howlett@deakin.edu.au

Y. Shekibi · A. F. Hollenkamp
CSIRO Energy Technology,
Bayview Avenue,
Clayton, Victoria 3800, Australia

L. Jin · J. M. Pringle
ARC Centre of Excellence for Electromaterials Science,
Department of Materials Engineering, Monash University,
Wellington Rd,
Clayton, Victoria 3800, Australia

D. R. MacFarlane
ARC Centre of Excellence for Electromaterials Science,
Department of Chemistry, Monash University,
Wellington Rd,
Clayton, Victoria 3800, Australia

Introduction

Plastic crystals in their solid form are a promising new type of electrolyte for electrochemical applications, particularly lithium ion batteries [1–10]. These materials are classified as fast ion conductors, where one ion (Li^+, for example, when present as a dopant ion) is able to move rapidly against a background of a relatively static matrix [8]. The name "plastic crystal" originates from the existence of long-range, ordered crystal structure together with frequent short-range rearrangements which leads to enhanced diffusivity and the ability to deform under an applied load [4, 11]. Although plastic crystals generally exhibit ionic conduction, those containing organic ionic species mostly based on cations of aliphatic or heterocyclic amines are often found to demonstrate remarkable conductivity at ambient temperatures, the so-called "organic ionic plastic crystal (OIPC)" materials. In principle, OIPCs can deliver high Li^+ ion transport number and plastic mechanical

properties, both of which should ideally translate into fast kinetics and good electrode–electrolyte contact as well as good accommodation of volume changes during charge–discharge cycling [6]. Moreover, doping of certain OIPCs with lithium salts of the same anion has been reported to enhance the conductivity by up to two orders of magnitude, creating the possibility of utilising these materials in practical charge storage devices [8, 10]. Solid-state electrolytes, such as OIPCs, also possess safety advantages in comparison to their liquid counterparts.

Whilst these advantages, particularly the very high conductivity once doped with lithium salts, were first noted back in the 1990s [10], the resistance of cells containing OIPC electrolytes is still too high for practical application. Nevertheless, our recent communication demonstrates that if a Li|OIPC|Li cell is charged and discharged for a certain number of cycles at low rates, then a conductive interfacial region, e.g. solid electrolyte interphase (SEI), is postulated to form between the lithium metal and the OIPC, such that the performance of the lithium half-cell was significantly improved, exhibiting stable cycling at reasonable current densities, and the resistivity of the cell was greatly diminished [12]. This observation together with our recent finding that a proper tuning on the cell interface, e.g. inclusion of separator and heating prior to operation results in remarkable improvements in lithium battery performance, has prompted our hypothesis that the electrode|electrolyte interface has a dominant role [13].

This paper focuses on the properties of lithium cells based on OIPCs at temperatures where the electrolyte exists predominantly as a solid, thus resulting in an all solid-state device as well as at somewhat elevated temperatures, where a liquid phase electrolyte supported by a polymer separator prevails. We discuss the role of separator, temperature and charge–discharge rate on the overall battery performance. The structures of the OIPCs discussed in this work are shown in Scheme 1.

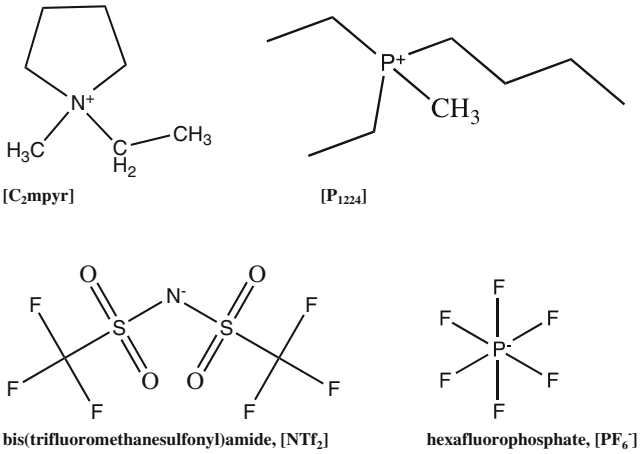

Scheme 1 The chemical structures and abbreviations of the cations and anions for the organic ionic plastic crystals utilised in this work

Experimental

The OIPC materials used in this work were prepared and purified according to published methods [14, 15]. Differential scanning calorimetry was performed using a TA-Q100 instrument. All samples were weighed (about 3 mg) and sealed in aluminium pans under N_2 atmosphere. The samples were first cooled down to −140 °C, followed by heating to 120 °C at a rate of 10 °C min^{-1}. A second repeated cooling and heating cycle was performed, and the thermal transitions reported were determined from the second heating traces.

A JEOL JCM-5000 (NeoScope) benchtop scanning electron microscope was used to probe the morphology of the cross-section of lithium symmetrical cells after cell cycling. The images were captured at 5 kV accelerating voltage on non-coated samples.

Solid-state electrolyte discs with varying thickness were prepared by pressing the particular OIPC powder using a KBr die (13-mm diameter) in a hydraulic press at 10 ton for 30 min. The OIPC disc was sandwiched between two lithium foils (Aldrich, 99.9% purity) and was assembled in a hermetic stainless steel test cell. The symmetrical cell configuration is used to study the Li|OIPC interfacial behaviour. All the assembly processes were performed in an argon glovebox. The symmetrical cells were placed inside a Faraday cage incorporating temperature control. A Princeton Applied Research VMP2/Z multichannel potentiostat (incorporating a frequency response analyser) was used for galvanostatic cycling at 0.01 mA cm^{-2} and impedance spectra measurement. The impedance spectra were collected in a frequency range of 10 MHz to 0.01 Hz using an alternating current bias of 0.1 V. All data was collected using EC-Lab software v9.97.

A stainless steel coin cell model CR2032A was used to assemble batteries using 12.7-mm-diameter disk $LiFePO_4$ cathode coated onto Al foil, a 12.7-mm-diameter disk lithium foil (China Energy Lithium, 0.33 mm thick, brushed with hexane prior to assembly) anode, a 10 mol% $LiNTf_2$-doped $[C_2mpyr][NTf_2]$ OIPC electrolyte and three different separators, e.g. Separion®, glass fibre and polyvinylidene fluoride (PVdF) separators. Both separators and cathodes were dried under vacuum at 100 °C for 2 days and cells were assembled in an argon-filled glove box. After drying, all materials were handled and stored in a high purity argon glovebox. The separator was then saturated with plastic crystal electrolyte by heating at 80°C for 2 h. The batteries were placed inside a Thermo Scientific T6030 oven and galvanostatically cycled using a Maccor series 4000 battery tester. A different current was used with a square wave profile and a 30 s rest step

between charge and discharge. The charge and discharge cut-off voltage was 3.6 and 3.0 V, respectively.

Results and discussion

Lithium metal symmetrical cell studies

In a lithium symmetrical cell, two identical lithium electrodes separated by an OIPC electrolyte are subjected to alternating charging and discharging (galvanostatic) cycles whilst monitoring the potential across the cell. The latter then provides a direct measure of the cell resistance and is comprised of contributions from the two interfacial regions (Li|OIPC) in addition to the bulk electrolyte. In our experiments, a cycling period of 1 h, at a current density of 0.01 mA cm^{-2} is used throughout. Our group has previously demonstrated that during the galvanostatic cycling of the symmetrical cell of Li|1 mol% $LiNTf_2$-doped $[C_2mpyr][NTf_2]$|Li, a substantial decrease of the potential bias occurs after 7–10 cycles [12]. We have described this behaviour in terms of a preconditioning process. The decrease in potential bias here suggests that reduced cell resistance, arguably due to improved lithium transport, takes place during the process since the potential bias reflects the cell resistance [at constant current density, potential bias follows Ohm's law ($V=IR$)]. This so-called "preconditioning behaviour" seems to be extendable to other OIPC systems from similar observations in cells incorporating *N*,*N* dimethylpyrrolidinium tetrafluoroborate, $[C_1mpyr][BF_4]$ and Triethyl(methyl)phosphonium *bis*(trifluoromethanesulfonyl)amide, $[P_{1222}][NTf_2]$ electrolytes [12, 13]. Figure 1 shows a similar phenomenon in a pure phosphonium cation-based plastic crystal, e.g., diethyl (methyl)(isobutyl)phosphonium hexafluorophosphate, $[P_{1224}][PF_6]$, on which a relatively steady potential bias is reached after eight charge–discharge cycles, again highlighting the general applicability of this process to OIPC with different cations and anions.

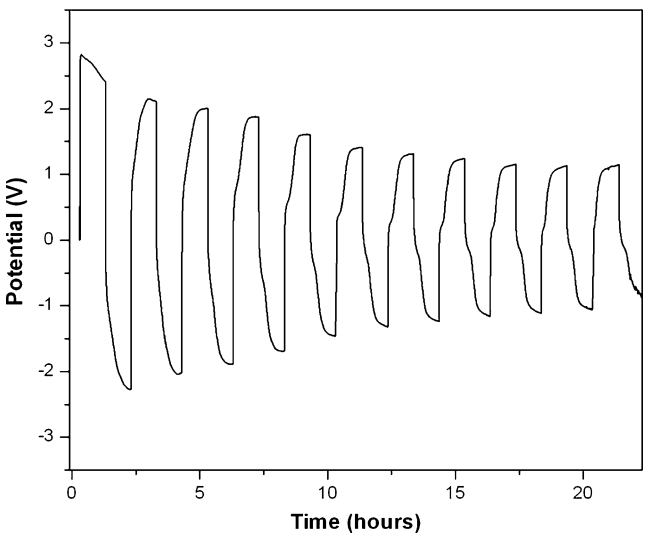

Fig. 1 Galvanostatic cycling response on a Li|$[P_{1224}][PF_6]$|Li cell using 330-μm-thick electrolyte at 50 °C

The typical effects of electrolyte thickness and temperature on the cell resistance and the required preconditioning time using 1 mol% $LiNTf_2$-doped $[C_2mpyr][NTf_2]$ electrolyte can be best illustrated using the composite Fig. 2. Figure 2a and b depicts the potential response to galvanostatic cycling and the sequential impedance spectra using a 100-μm-thick electrolyte at 50 °C; Fig. 2c and d depicts the potential response to galvanostatic cycling and the sequential impedance spectra using a 200-μm-thick electrolyte at 50 °C; Fig. 2e depicts the potential response to galvanostatic cycling using a 200-μm-thick electrolyte at 25 °C, and Fig. 2f depicts the thermal phase evolution of the electrolyte. Figure 2a and c shows a large initial potential bias, indicating a substantial resistance which subsequently falls dramatically over the first 20 cycles. This behaviour is remarkably similar to that observed by Bhatt et al. in their study of lithium symmetrical cells with *N*-propyl-*N*-methylpyrrolidinium bis(fluorosulfonyl)amide ($[C_3mpyr][FSI]$) ionic liquids, in which they attributed the behaviour to the decrease in the interfacial resistance that accompanies the establishment of an effective SEI [16]. The fact that both cells (100 and 200 μm) initially have almost identical resistance again implies that interfacial resistance dominates. The decrease of potential bias with increasing cycles (and time) also coincides with the decreasing impedance arc over increasing cycles shown in the sequential electrochemical impedance spectra (Fig. 2b and d). Both cells ultimately reach a steady state (constant potential bias magnitude and impedance response) as the effect of SEI resistance progressively decreases. At this point, cell resistance is largely determined by the conductivity of the bulk electrolyte. Hence, the steady-state potential bias for the 200-μm cell is approximately twice that of the 100-μm cell (compare Fig. 2a and c). Temperature change, however, substantially alters both the potential bias magnitude and the transient period (compare Fig. 2c and e). Lowering temperature from 50 °C to 25 °C, for example, results in the more-than-double increase in potential bias (both the initial and steady ones) with ~340 h cycling period is required to reach the steady state. The increased potential bias is directly related to the fact that, at 25 °C, the electrolyte exists in phase II with the conductivity of 4×10^{-7} Ω^{-1} cm^{-1}, whilst at 50 °C, the electrolyte is in phase I with the larger conductivity of 1×10^{-6} Ω^{-1} cm^{-1} (Fig. 2f) [9]. Given that SEI formation requires significant diffusion of ions from the bulk electrolyte, it is not surprising that the preconditioning period (transition through SEI formation to steady state) is considerably longer at the lower temperature.

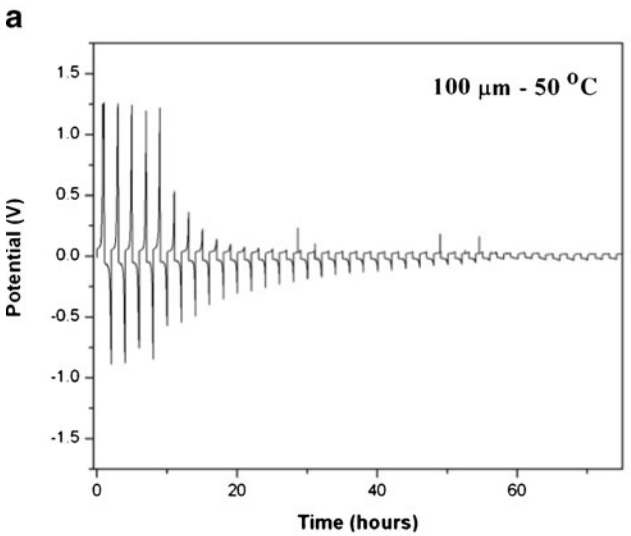
a
100 μm - 50 °C
Potential (V)
Time (hours)

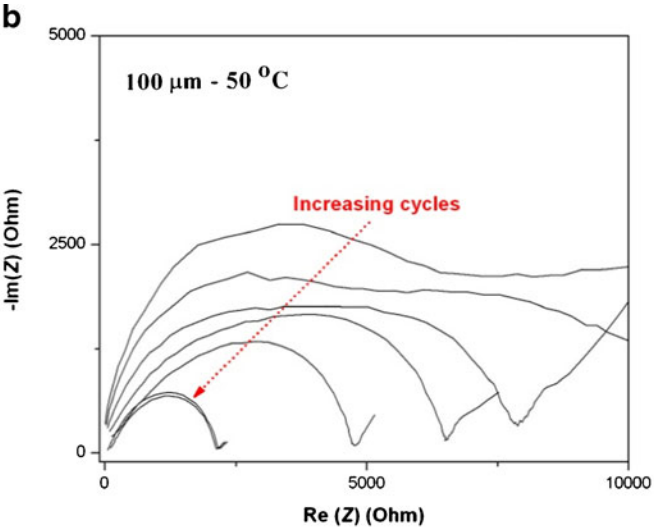
b
100 μm - 50 °C
Increasing cycles
-Im(Z) (Ohm)
Re (Z) (Ohm)

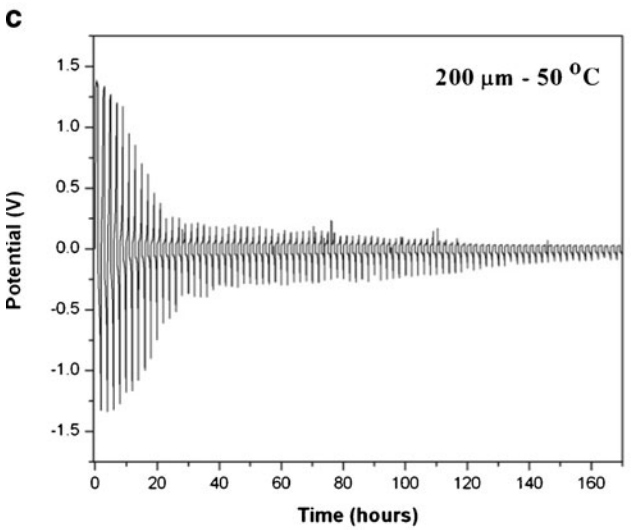
c
200 μm - 50 °C
Potential (V)
Time (hours)

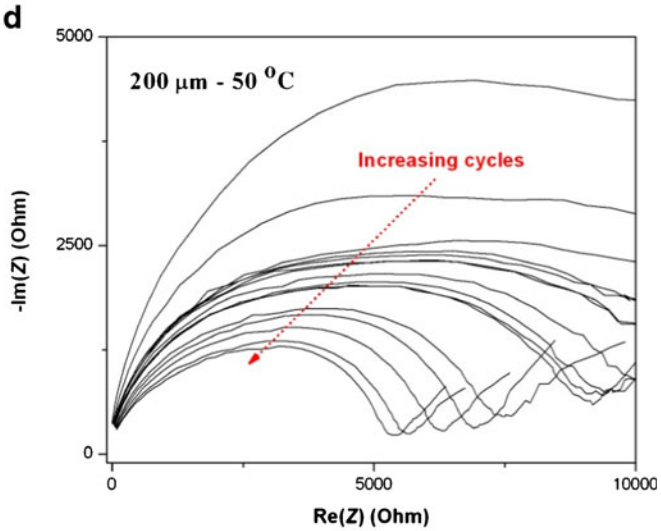
d
200 μm - 50 °C
Increasing cycles
-Im(Z) (Ohm)
Re(Z) (Ohm)

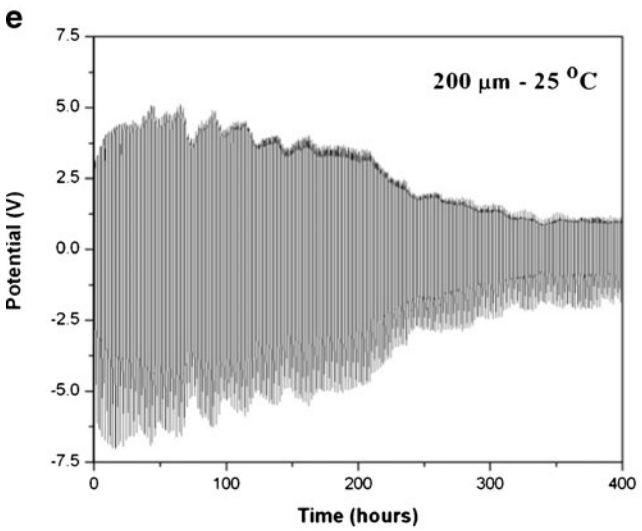
e
200 μm - 25 °C
Potential (V)
Time (hours)

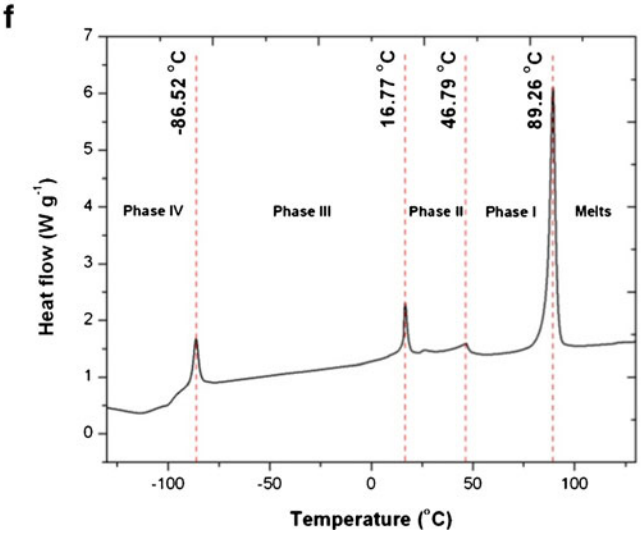
f
-86.52 °C
16.77 °C
46.79 °C
89.26 °C
Phase IV
Phase III
Phase II
Phase I
Melts
Heat flow (W g-1)
Temperature (°C)

◀ **Fig. 2** Data acquired from a Li|1 mol% $LiNTf_2$-doped $[C_2mpyr][NTf_2]$|Li cell. **a** Potential response to galvanostatic cycling (0.01 mA cm^{-2}). **b** Sequential impedance spectra from a 100-μm-thick electrolyte at 50 °C. **c** Potential response to galvanostatic cycling (0.01 mA cm^{-2}). **d** Sequential impedance spectra from a 200-μm-thick electrolyte at 50 °C. **e** Potential response to galvanostatic cycling (0.01 mA cm^{-2}) for a 200-μm-thick electrolyte at 25 °C. **f** Differential scanning calorimetry data for 1 mol% $LiNTf_2$-doped $[C_2mpyr][NTf_2]$

The beneficial effect of preconditioning cycles on the lithium transport properties is closely associated with the modification in the OIPC surface during cycling, e.g. reduction of grain size at the interface and the respective increased volume of grain boundaries which is normally considered to exist in a more disordered phase relative to the grain phase; this was observed previously in symmetrical cells incorporating $[C_2mpyr][NTf_2]$ and $[C_1mpyr][BF_4]$ [12, 13]. Further supporting evidence is presented in Fig. 3 which displays the scanning electron microscopy image of the Li|electrolyte interface on the cell subjected to cycling at 50 °C and current density of 0.01 mA cm^{-2} for 6 months. No sharp boundary between the lithium and the electrolyte is observed here. In particular, the formation of thick laminated structure (different to the bulk electrolyte) is evident in the OIPC electrolyte layer directly adjacent to the interface; indicating that an extensive SEI layer has been formed and good contact between lithium and electrolyte surfaces is achieved.

After inducing the preconditioning effect using a 0.01 mA cm^{-2} current, there is an upper limit value which can be determined by varying the current and studying the potential response. This is shown, for example, in the case of a 1 mol% $LiNTf_2$-doped $[C_2mpyr][NTf_2]$ electrolyte in a symmetrical cell after reaching steady state (Fig. 4a) using 10–500 μA cm^{-2} current density. Between 10 and 300 μA, a proportional increase in the potential value with increasing current density is apparent. On the other hand, applying a current density in excess of 300 μA cm^{-2} immediately leads to a large deviation from this relationship, clearly demonstrated in Fig. 4b, which plots the ratio of peak potential to the applied current obtained from the 3 rd charging profile. The deviation from the linear regression line representing constant resistance (Ohmic behaviour) is likely to indicate the occurrence of irreversible processes related to electrolyte decomposition. Thus, for 1 mol% $LiNTf_2$, using current density below the level that the material can sustain (e.g. 300 μA cm^{-2}), is more practical.

Li metal–$LiFePO_4$ cell studies

Good battery performance necessitates sufficiently high lithium ionic conductivity in the bulk electrolyte as well as the supply of lithium ions at both cathode|electrolyte and lithium metal anode|electrolyte interfaces to sustain fast charge–discharge processes [1]. Lithium salt concentration plays an important role in this regard, with a typical concentration of ~0.3 mol kg^{-1} regarded as the lowest optimum concentration in traditional solvents or ionic liquids [1]. Therefore, a lithium salt (e.g. $LiNTf_2$) concentration of 10 mol% is utilised in the battery cell study here, which corresponds to a concentration of ~0.26 mol kg^{-1}. Figure 5 presents results of parameter studies in $LiFePO_4$| 10 mol% $LiNTf_2$-doped $[C_2mpyr][NTf_2]$|Li cells.

The use of separator and its choice is often an overlooked yet apparently essential aspect towards achieving high-performing OIPC-based batteries. Perfect coverage of the solid electrolyte onto the electrode surfaces is necessary to attain fast charge–discharge interfacial reactions. This can be simply achieved by partially or completely melting the OIPC onto the electrode surfaces by heating to temperatures near or at its melting point. The separator is thus essential here to prevent direct contact between electrodes during cooling (e.g. solidification) process or when operating at an elevated temperature where the OIPC may exist in

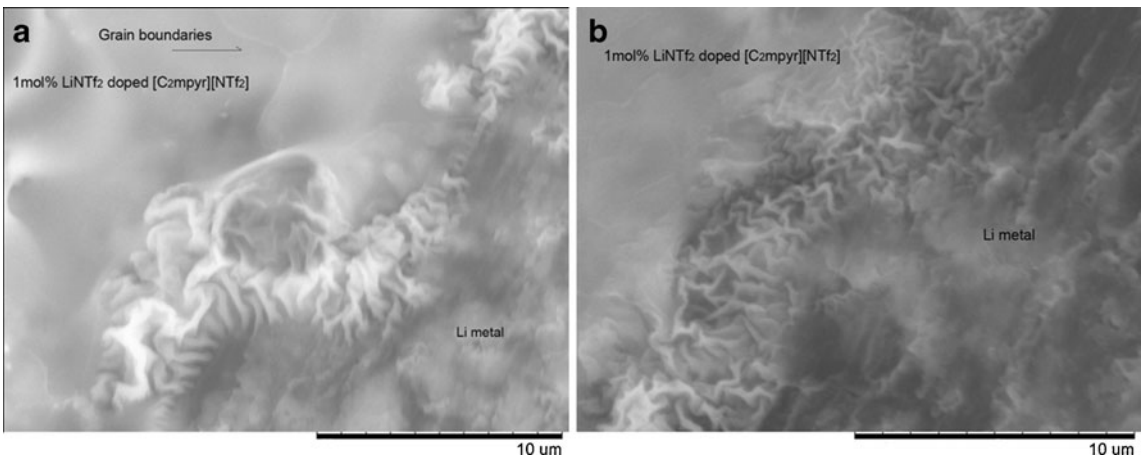

Fig. 3 Scanning electron microscopy images of the Li|$[C_2mpyr][NTf_2]$ interface at different magnifications **a** 7,000× and **b** 8,000× after cycling for 6 months

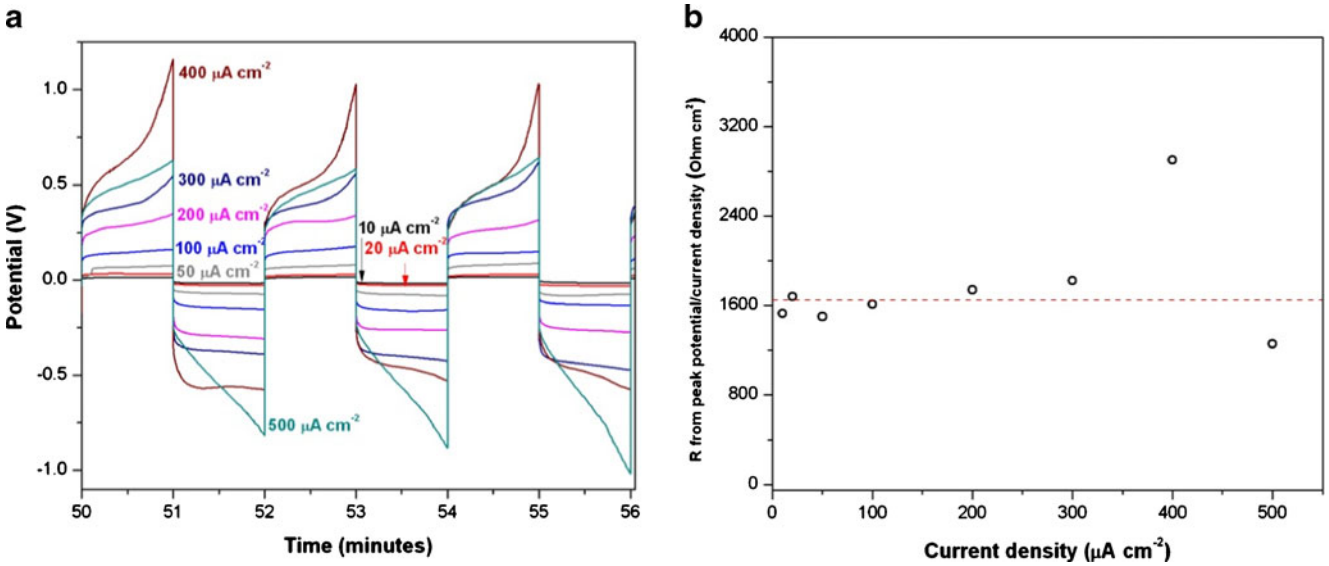

Fig. 4 **a** Steady-state galvanostatic cycling response of a Li|1 mol% $LiNTf_2$-doped $[C_2mpyr][NTf_2]$|Li cell at 50 °C (100-μm-thick electrolyte) and different applied current density. **b** Ratio of peak potential to applied current density from the 3 rd charging profile as a function of applied current density

at least a partially molten state. In addition, during long charge–discharge cycling, localised hot spots in the electode|electrolyte interface might result in the partial melting of the electrolyte and thereby cause shorting. For doped $[C_2mpyr][NTf_2]$ operated at or below 80 °C, three separator options were considered, e.g. commercially available Separion®, glass fibre and PvdF separators. Separion® shows better capacity performance over increasing cycles relative to glass fibre at 80 °C and 0.1 C current discharge rate (Fig. 5a). Nonetheless, superior performance is attained using PvdF as evidenced by larger capacity at higher current rate at any given temperature (Fig. 5b). Therefore, we have chosen this latter separator for subsequent battery studies in this work. The wetting compatibility between the separator and the OIPC seems to determine the cell performance as suggested by the similar order on which the wetting is improved, e.g. glass fibre, Separion® and PvdF.

The performance of a lithium cell incorporating PvdF separator over 20 and 110 cycles is shown in Fig. 5b and c, respectively. An increase in temperature translates to improved discharge capacity and cathode utilisation (Fig. 5b). At 0.2 C current, the median discharge capacity is improved from 121 to 131 mAh g^{-1} and then to 153 mAh g^{-1} by increasing the temperature from 50 °C to 60 °C and then to 80 °C, respectively. Accordingly, the cathode utilisation also rises from 71% to 77% and then to 90% (when 170 mAh g^{-1} is taken as the full capacity of $LiFePO_4$). It is worthy to note here that at 50 °C and 60 °C, the electrolyte remains in its predominant solid form, whilst at 80 °C, the electrolyte exists in its molten form as indicated in Fig. 5d. The benefits of operating at 80 °C in ionic liquid form are evident in terms of active material utilisation, particularly at higher current rate. Increasing the current from 0.2 C to 0.5 C, for example, leads to a very minor median capacity deterioration of only 3% (e.g. 153 to 149 mAh g^{-1}; Fig. 5b). This observation is in marked contrast with similar OIPC (e.g. 20 mol% $LiNTf_2$-doped 5-methyl-5,6,7,8-tetrahydro-pyrazolo pyridazin-4-ium *bis*(trifluoromethanesulfonyl)amide)-based battery cell operated at 40 °C, which showed ~19% capacity reduction upon increasing the rate from 0.25 C to 0.5 C [5]. Another striking feature of operating at 80 °C is the excellent stability as demonstrated in Fig. 5c. After some mild capacity fluctuations during the initial cycles, approximately 15 cycles, no appreciable drop is noticed over the following 110 cycles. For the same cell operated at 50 °C at a rate of 0.2 C, however, a substantial capacity drop is observed after similar cycling. These characteristics undoubtedly provide great promise for the future of higher than ambient temperature batteries, especially accounting for the fact that such devices are still in their developmental stage.

The typical potential versus capacity at 80 °C for the 4th, 50th and 100th cycles at a 0.2 C rate is depicted in Fig. 5e.

Fig. 5 Data acquired from a Li|10 mol% $LiNTf_2$-doped $[C_2mpyr][NTf_2]$|$LiFePO_4$ cell. **a** Discharge capacity versus cycle number for the first 20 cycles using separion and glass fibre separators. **b** Discharge capacity versus cycle number for the first 20 cycles using PvdF separator. **c** Discharge capacity versus cycle number for the first 110 cycles PvdF separator. **d** Differential scanning calorimetry data for 10 mol% $LiNTf_2$-doped $[C_2mpyr][NTf_2]$. **e** Potential versus capacity using PvdF separator at 80 °C. **f** Initial potential response at different current at 80 °C

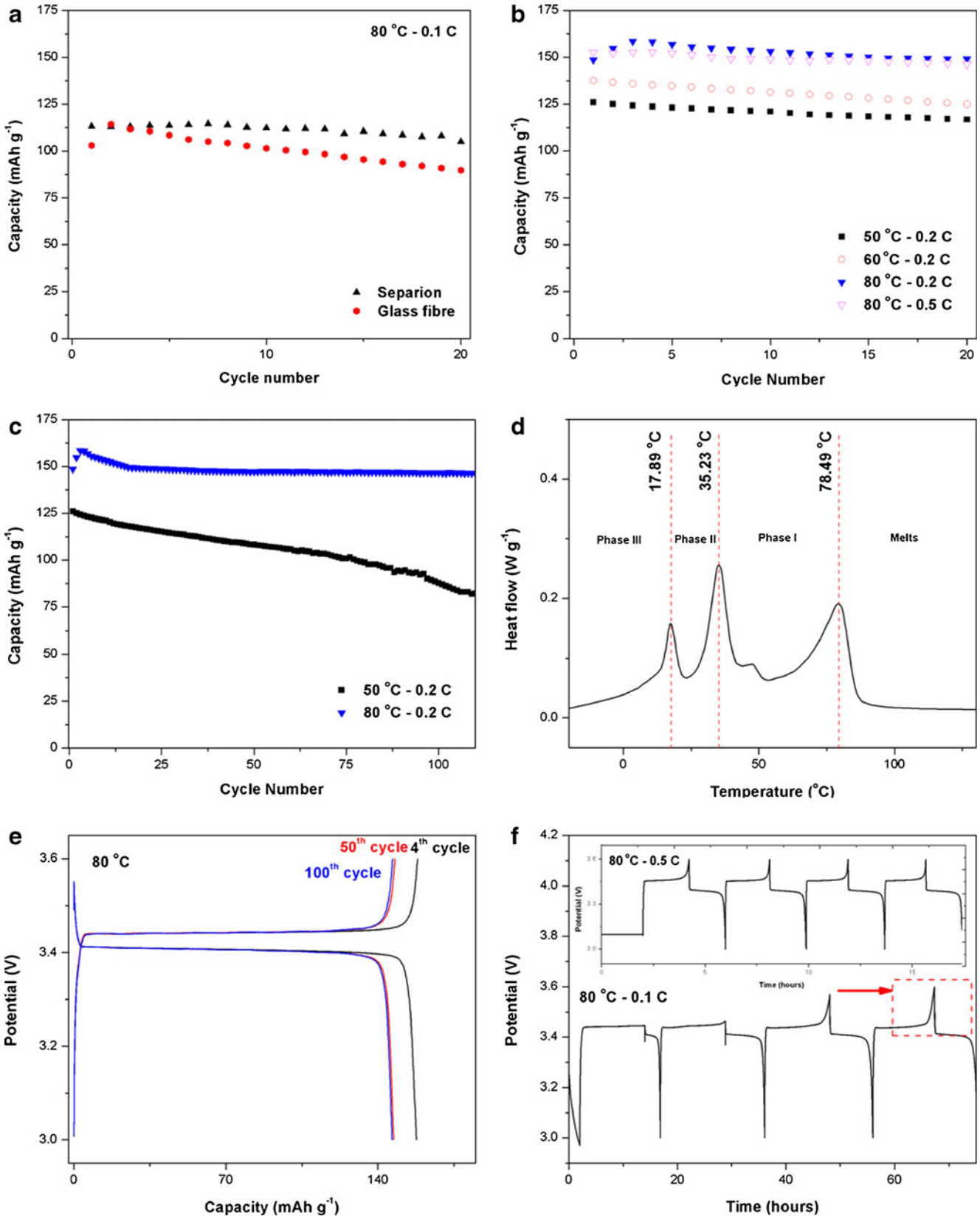
a
80 °C - 0.1 C
Capacity (mAh g-1)
Cycle number
Separion
Glass fibre
b
50 °C - 0.2 C
60 °C - 0.2 C
80 °C - 0.2 C
80 °C - 0.5 C
Capacity (mAh g-1)
Cycle Number
c
50 °C - 0.2 C
80 °C - 0.2 C
Capacity (mAh g-1)
Cycle Number
d
17.89 °C
35.23 °C
78.49 °C
Phase III
Phase II
Phase I
Melts
Heat flow (W g-1)
Temperature (°C)
e
80 °C
50th cycle
4th cycle
100th cycle
Potential (V)
Capacity (mAh g-1)
f
80 °C - 0.5 C
Potential (V)
Time (hours)
80 °C - 0.1 C
Potential (V)
Time (hours)

The substantial drop in capacity from the 4th cycle to 50th cycle is consistent with the initial capacity fluctuation with potential peaks around the 4th cycle (Fig. 5b). It is evident that there is only slight capacity drop between the 50th to 100th cycle. In addition, the efficiency, i.e. the ratio of charge-to-discharge capacity, increases from 99.63% (4th cycle) to 99.68% (50th cycle) and then to 99.88% (100th cycle).

Our observations of the preconditioning process in lithium symmetrical cell studies presented earlier can be seen to extend to full battery cell studies (Fig. 5f). This figure shows the potential response on two different battery cells subjected to very initial charge–discharge cycling at 80 °C directly after their assemblies and at different rates of 0.1 C (main) and 0.5 C (inset). Interestingly, the cell cycled at low current of 0.1 C does not achieve the upper potential limit immediately during the first three cycles, indicating that the full charging capacity of the cell is not reached. However, discharge capacity increases consistently throughout these cycles, implying that SEI formation is occurring within these initial cycles. This behaviour, however, does not occur in the cell cycled at high currents of 0.5 C, since the upper limit is readily attained in the 1st cycle and the discharge capacity remains constant throughout. This latter observation has prompted us to think that, in the high current (fast charge and discharge) mode, either the SEI is formed rapidly or another mechanism prevails which would become the focus of our future studies.

Conclusions

We have previously demonstrated that OIPC electrolytes can enable solid-state lithium metal cells with high stability following an initialising or preconditioning period. This paper provides additional evidence on the general nature of the preconditioning process (i.e. the charging and discharging processes) which leads to a progressive fall in cell resistance in lithium symmetrical cells using OIPC electrolytes. We also postulate that during the process, initially, the resistance is dominated by the interface, and as the cycling process continues, the bulk electrolyte begins to contribute before eventually fully dominating when steady state is reached. This mechanism, in turn, explains the longer transient period and higher steady-state potential bias observed at lower temperature (at 25 °C relative to those at 50 °C) as well as similar transient period and half-reduction in steady-state potential bias noticed when the original electrolyte thickness (200 μm) is reduced by half. We also show that at a current density above 300 mA cm^{-2}, the preconditioning response does not follow Ohmic behaviour, implying that this current magnitude is the upper limit for the [C_2mpyr][NTf_2] OIPC.

This work also demonstrates that the nature of the separator substantially affects OIPC-based battery performance. At operating temperatures of 80 °C and below using 10 mol% LiNTf_2-doped [C_2mpyr][NTf_2], the discharge capacity decreases in the order of the cells containing PvdF, Separion® and glass-fibre separators, respectively. The battery cell with PvdF separator delivers discharge capacity up to 126 and 137 mAh g^{-1} at 50 °C and 60 °C, respectively, when the electrolyte is in its solid form. At higher temperature of 80 °C in the liquid form, an even larger discharge capacity up to 153 mAh g^{-1} is demonstrated. Whilst operating at 50 °C and 60 °C led to constant capacity reduction over increasing cycles, very stable capacity is maintained for over 110 cycles when operating at 80 °C. Moreover, increasing the current from 0.2 C to 0.5 C resulted in only a slight capacity reduction from 153 to 149 mAh g^{-1}.

Acknowledgements The authors gratefully acknowledge the financial support from the Australian Research Council (ARC) through the ARC Centre of Excellence for Electromaterials Science and ARC Laureate Fellowship for Maria Forsyth. Jaka Sunarso acknowledges Alfred Deakin Postdoctoral Research Fellowship from Deakin University.

References

1. Seki S, Ohno Y, Kobayashi Y, Miyashiro H, Usami A, Mita Y, Tokuda H, Watanabe M, Hayamizu K, Tsuzuki S, Hattori M, Terada N (2007) J Electrochem Soc 154:A173–A177
2. Zhou Z-B, Matsumoto H (2007) Electrochem Commun 9:1017–1022
3. Abouimrane A, Whitfield PS, Niketic S, Davidson IJ (2007) J Power Sources 174:883–888
4. Abouimrane A, Abu-Lebdeh Y, Alarco P-J, Armand M (2004) J Electrochem Soc 151:A1028–A1031
5. Alarco P-J, Abu-Lebdeh Y, Ravet N, Armand M (2004) Solid State Ionics 172:53–56
6. Abu-Lebdeh Y, Abouimrane A, Alarco P-J, Armand M (2006) J Power Sources 154:255–261
7. MacFarlane DR, Meakin P, Amini N, Forsyth M (2001) J Phys Condens Matter 13:8257–8267
8. MacFarlane DR, Forsyth M (2001) Adv Mater 13:957–966
9. Forsyth M, Huang JH, MacFarlane DR (2000) J Mater Chem 10:2259–2265
10. MacFarlane DR, Huang J, Forsyth M (1999) Nature 402:792–794
11. Annat G, Adebahr J, McKinnon IR, MacFarlane DR, Forsyth M (2007) Solid State Ionics 178:1065–1071
12. Howlett PC, Shekibi Y, MacFarlane DR, Forsyth M (2009) Adv Eng Mater 11:1044–1048
13. Howlett PC, Sunarso J, Shekibi Y, Wasser E, Jin L, Kar M, MacFarlane D, Forsyth M (2011) Solid State Ionics (submitted for publication)
14. Armel V, Velayutham D, Sun J, Howlett PC, Forsyth M, MacFarlane DR, Pringle JM (2011) J Mater Chem 21:7640–7650
15. MacFarlane D, Meakin P, Sun J, Amini N, Forsyth M (1999) J Phys Chem B 103:4164–4170
16. Bhatt AI, Best AS, Huang J, Hollenkamp AF (2010) J Electrochem Soc 157:A66–A74